

Ferroelectricity and superconductivity in strained $\text{Eu}_x\text{Sr}_{1-x}\text{TiO}_3$ films

Nicholas G. Combs , Hanbyeol Jeong , Ryan Russell, Linus Kautzsch , Tyler N. Pardue, Thomas E. Mates, Stephen D. Wilson, John W. Harter , and Susanne Stemmer *

Materials Department, University of California, Santa Barbara, Santa Barbara, California 93106-5050, USA

 (Received 4 January 2023; revised 8 February 2023; accepted 21 February 2023; published 6 March 2023)

The superconducting transition of SrTiO_3 can be influenced by tuning its ferroelectric transition, but the underlying reasons remain poorly understood. Here, we investigate compressively strained, Sm-doped films of $\text{Eu}_x\text{Sr}_{1-x}\text{TiO}_3$ that were grown by molecular beam epitaxy to determine the effect of alloying with Eu on both superconductivity and ferroelectricity, both of which are present in strained SrTiO_3 films. Remarkably, superconductivity survives up to $x = 0.14$. Films at the lowest alloy concentration studied here, $x = 0.09$, exhibit no suppression of their superconducting transition temperature, but there is a strong reduction of the upper critical field (H_{c2}), compared to nonalloyed, strained SrTiO_3 films. In addition, these films lack the sharp ferroelectric transition that appears in films without Eu in second harmonic generation measurements. We postulate that Eu alloying causes a crossover from a globally ordered ferroelectric state to one with only short-range polar order. We discuss the connection between the loss of global polar order and the change in the superconducting properties.

DOI: [10.1103/PhysRevB.107.094504](https://doi.org/10.1103/PhysRevB.107.094504)

I. INTRODUCTION

Superconductivity in electron-doped SrTiO_3 was discovered in 1964 [1], and yet the nature of its superconducting pairing mechanism remains debated to this day [2]. Superconductivity in SrTiO_3 persists to very low carrier densities, which challenges the applicability of standard Bardeen-Cooper-Schrieffer (BCS) theory due to the Fermi energy being much lower than its Debye energy [1,3]. Additionally, bulk, pure SrTiO_3 is an incipient ferroelectric [4]. Recently, there has been significant interest in finding a possible link between the superconducting state and the incipient ferroelectricity [5–9]. While many theories so far have focused on superconductivity emerging from a paraelectric (i.e., centrosymmetric) state, fewer have considered the possibility of superconductivity emerging from a ferroelectric or polar phase, which is characterized by the presence of broken inversion symmetry.

Numerous approaches can be used to tune SrTiO_3 into the ferroelectric state, such as Ca, Ba, and isotopic ^{18}O substitution [10–13] and stress [14], including epitaxial coherency strains [15,16]. When electron doping is also present, these methods have demonstrated an enhancement of the superconducting transition temperature T_c above that of the unstrained SrTiO_3 with comparable carrier densities [11,17–22]. This is sometimes interpreted as the result of a ferroelectric quantum critical point whose fluctuations putatively lead to Cooper pairing. This picture is, however, in contrast with the fact that in many of these studies, superconductivity emerges from a polar ground state [11,18,21,22]. Indeed,

some of the highest reported T_c 's have been observed in samples that were already strongly in the polar regime upon entering the superconducting state [18,21,22]. Additionally, in strained films, suppression of superconductivity has been correlated to the destruction of the (global) ferroelectric state, either by overdoping [21,22] or by decreasing the film thickness [23]. Moreover, even nominally paraelectric SrTiO_3 can be locally polar [24–26]. A number of scenarios of locally polar states have been suggested, such as dynamic off-centering of the polarizable Ti ion [27] or polar regions that cluster around impurity atoms in a highly polarizable lattice [28–30]. Recently, however, high-resolution scanning transmission electron microscopy (STEM) has shown evidence of *static* polar nanodomains in the paraelectric phase [26,31,32].

Superconductivity in SrTiO_3 films exhibits other peculiarities as well. These include upper critical fields (H_{c2}) that exceed the paramagnetic (Pauli or Clogston-Chandrasekhar) limit [33–35] and an apparent insensitivity of T_c to the presence of magnetic impurities [21,34,36], in apparent contradiction of the Abrikosov-Gor'kov (AG) theory of paramagnetic impurities in an *s*-wave superconductor [37]. Although each of these observations can have a trivial explanation, such as thin film or multiband effects [34,38,39], another possibility is the effect of antisymmetric spin-orbit coupling (ASOC) induced by broken inversion symmetry on superconductivity [40–45]. An important role of spin-orbit coupling, present in noncentrosymmetric materials, was already suggested in studies of $\text{LaAlO}_3/\text{SrTiO}_3$ samples, whose T_c appears linked to the strength of Rashba-like ASOC [46–48]. Going further, it has even been suggested that topological superconductivity may be found in noncentrosymmetric SrTiO_3 -based systems [49–51]. All of these observations strongly suggest that the role of broken inversion symmetry and spin-orbit coupling in

*Corresponding author: stemmer@mrl.ucsb.edu

the superconducting state of SrTiO₃ deserve further investigation.

In this study, we investigate alloys between SrTiO₃ and EuTiO₃. Previously, it was shown that alloying strained SrTiO₃ with magnetic Eu²⁺ up to concentrations of 3% produced essentially no change in the superconducting properties. Due to the almost identical ionic radii of Sr²⁺ and Eu²⁺, which leads to the end members SrTiO₃ and EuTiO₃ having identical bulk lattice constants, the Eu_xSr_{1-x}TiO₃ system presents a unique playground for exploring the effects of alloying without changing the strain state of the films. Both superconductivity and ferroelectricity must be expected to disappear at some concentration x (though not necessarily the same x), as EuTiO₃ is not a superconductor and, at the compressive strain levels used here, it is also not ferroelectric [52]. Here, we show that superconductivity does eventually become suppressed by Eu alloying. Interestingly, our data indicate that this does not seem to be brought about by magnetic (dis)order, but rather by a reduction of polarizability of the lattice, as told by suppression of the ferroelectric transition and polar nanodomains.

II. EXPERIMENT

Coherently strained, Sm-doped EuTiO₃/Eu_xSr_{1-x}TiO₃ heterostructures were grown on (001) (LaAlO₃)_{0.3}(Sr₂AlTaO₆)_{0.7} (LSAT) crystal substrates by hybrid molecular beam epitaxy, as described elsewhere [53–55]. The LSAT substrate introduces a compressive in-plane strain of $\sim 0.9\%$ in both layers, while the thin (10 nm) Sm:EuTiO₃ cap prevents issues with surface depletion in relatively thin (70–100 nm) Eu_xSr_{1-x}TiO₃ layers, whose thickness is limited by the need to prevent strain relaxation [55,56]. The Sm dopant cell temperature was kept constant for all layers in a sample. Results from two series of films are presented in the main text. In the first series (series A), the alloy concentration of Eu in the Sm:Eu_xSr_{1-x}TiO₃ layer was kept constant at a nominal value of $x = 0.05$ (5% Eu) and the Sm³⁺ dopant concentration was varied. In the second series (series B), the Sm³⁺ dopant concentration was kept nominally constant in the optimally doped range (determined by the doping density of the sample in series A that produced the highest superconducting T_c) and x was varied. The nominal Eu concentration was estimated by the ratio of Sr/Eu beam equivalent pressures (BEPs) used during growth and corresponded to $x = 0.05$, 0.10, and 0.20 for series B. The relative Sr/Eu stoichiometry of the films was also determined by x-ray photoelectron spectroscopy (XPS), which estimated the stoichiometry of these to be closer to $x = 0.09$, 0.14, and 0.30, respectively (see Supplemental Material [56], which also contains Refs. [57–62]). Note that the optimally doped sample from series A (sample A3) is also used as the $x = 0.09$ sample in series B (sample B1). Summaries of film parameters and measured properties are presented in Tables I–III.

On-axis x-ray diffraction (XRD) measurements were carried out using a Philips Panalytical X’pert thin film x-ray diffractometer to assess out of plane lattice parameters and film thicknesses via Laue thickness fringes. The evolution of ferroelectric order was measured using optical second harmonic generation (SHG) from 10 to 200 K. Ultrafast laser

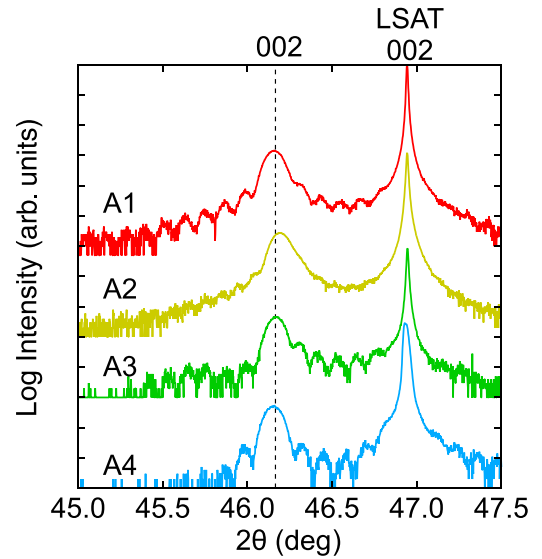


FIG. 1. XRD for series A films. The dotted line represents the fully strained, stoichiometric 002 lattice parameter.

pulses with 800 nm center wavelength, 40 fs duration, and 10 kHz repetition rate were focused to a spot size of 30 μm , as described previously [22]. Each point shown is the average of many points taken continuously as the temperature is changed. The SHG intensity shown is the average of the points within a chosen temperature interval.

Al shadow masks were used to deposit Ti(50 nm)/Au(250 nm) Ohmic contacts on the corners of the sample by electron beam evaporation. Sheet resistance (R_s), Hall carrier density (n_{3D}), and Hall mobility (μ) were measured from 300 to 2 K in van der Pauw (vdP) geometry using a Quantum Design Dynacool system. Longitudinal resistance (R) measurements between 14 mK and 1 K were performed in a dilution refrigerator (Oxford Instruments Triton) using low-frequency lock-in techniques. The superconducting transition temperature T_c was defined as the temperature at which $R/R_n = 0.05$, where R_n is the resistance measured at 1 K. Upper critical field (H_{c2}) measurements at 20 mK were performed on the series A samples with the highest measured T_c values. Sample A1 was measured with \mathbf{H} oriented out of the plane of the sample (oop), while samples A2 and A3 were measured with \mathbf{H} oriented in the plane of the sample (ip) (i.e., $\mathbf{H} \parallel \mathbf{n}$ and $\mathbf{H} \perp \mathbf{n}$, respectively, where \mathbf{n} is the film surface normal). Here H_{c2} is defined as the field at which $R/R_n = 0.5$. Only one orientation of H_{c2} was measured for each sample due to sample degradation between scans (see Supplemental Material for details [56]).

III. RESULTS

Results from the XRD measurements for series A films are shown in Fig. 1. All exhibit a single 002 film peak indicating that both the Sm:EuTiO₃ cap and the Sm:Eu_xSr_{1-x}TiO₃ are fully strained to the LSAT substrate, with the out of plane lattice parameter a_{op} close to the value expected for fully strained, stoichiometric films ($a_{op} = 3.930 \pm 0.001 \text{ \AA}$). Laue fringes indicate good crystallinity and smooth surfaces of the

TABLE I. Summary of properties for series A samples. The Sm:Eu_xSr_{1-x}TiO₃ thickness was measured via XRD thickness fringes and subtracting the estimated thickness of the Sm:EuTiO₃ capping layer.

Sample	n_{RT} (cm ⁻³)	Eu _x Sr _{1-x} TiO ₃ film thickness (nm)	T_c (mK)
A1	6.3×10^{19}	68	290
A2	7.4×10^{19}	92	330
A3	9.8×10^{19}	75	400
A4	1.2×10^{20}	68	75

heterostructures. The exception is sample A2, which exhibits a small degree of strain relaxation ($a_{op} \approx 3.927 \text{ \AA}$). The strain relaxation in A2 causes the slight dampening of the Laue thickness fringes, which are stronger in the other samples. The period of the thickness fringes corresponds to the total thickness of the heterostructure, and the measured thickness values for the Sm:Eu_xSr_{1-x}TiO₃ layer are given in Table I, after subtracting the estimated thickness of the Sm:EuTiO₃ capping layer. A representative reciprocal space map of sample A4 is included in the Supplemental Material [56].

The room temperature three-dimensional (3D) carrier density values n_{RT} for the series A films were calculated from

the Hall resistance, using the total heterostructure thickness as both layers contribute to conduction in the normal state [55]. The n_{RT} values were estimated to be $6.3 \times 10^{19} \text{ cm}^{-3}$, $7.4 \times 10^{19} \text{ cm}^{-3}$, $9.8 \times 10^{19} \text{ cm}^{-3}$, and $1.2 \times 10^{20} \text{ cm}^{-3}$ for samples A1–A4, respectively (Table I). Figure 2(a) shows R_s as a function of temperature (T) for series A films, all of which exhibit metallic behavior down to 2 K. In Fig. 2(b), the slight upturn in R_s around ~ 7 –8 K followed by a downward kink reflects conduction in the Sm:EuTiO₃ layer as it goes through an antiferromagnetic transition [54,63], indicative of parallel conduction in both the Sm:EuTiO₃ and Sm:Eu_xSr_{1-x}TiO₃ layers. Figure 2(c) shows n_{3D} as a function of temperature. An abrupt downturn in $n_{3D}(T)$ starting around ~ 100 K is observed in all films, which has been attributed to the ferroelectric transition causing localization of some fraction of the mobile carriers needed to screen the polarization [21,22]. The Hall mobility μ at low temperatures roughly scales with n_{RT} as seen in Fig. 2(d), consistent with ionized impurity scattering. The normal state transport behavior exhibited by the films mimics that of comparable heterostructures with 0% Eu [55], indicating that the presence of 9% Eu has minimal effects on the normal state transport properties.

Figure 3(a) shows R/R_n for the series A samples A1–A3. The measurement for sample A4 is shown separately in Fig. 3(b). The extracted T_c values as a function of n_{RT}

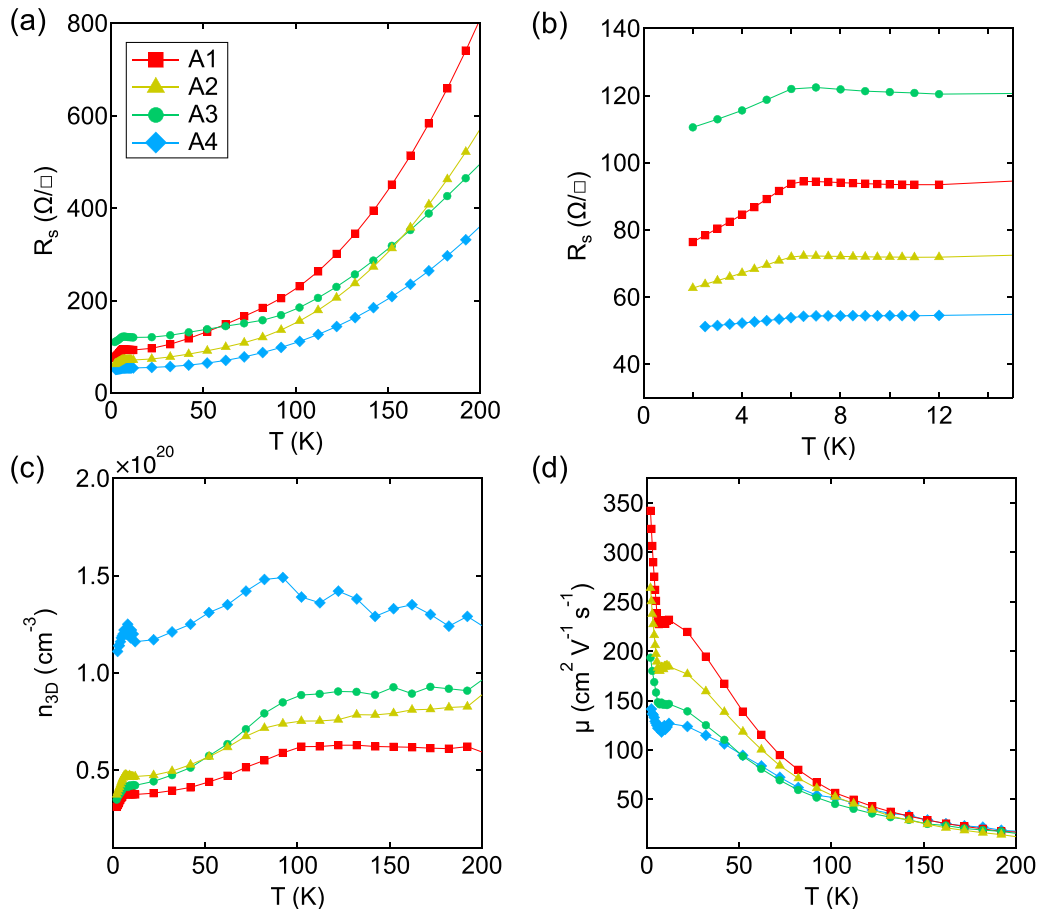


FIG. 2. Normal state transport measurements for series A films. (a) Sheet resistance R_s from 200 to 2 K; (b) zoomed in R_s below 15 K, showing the kink at the Néel temperature T_N of the Sm:EuTiO₃ capping layer. (c) n_{3D} as a function of temperature and (d) mobility μ as a function of temperature.

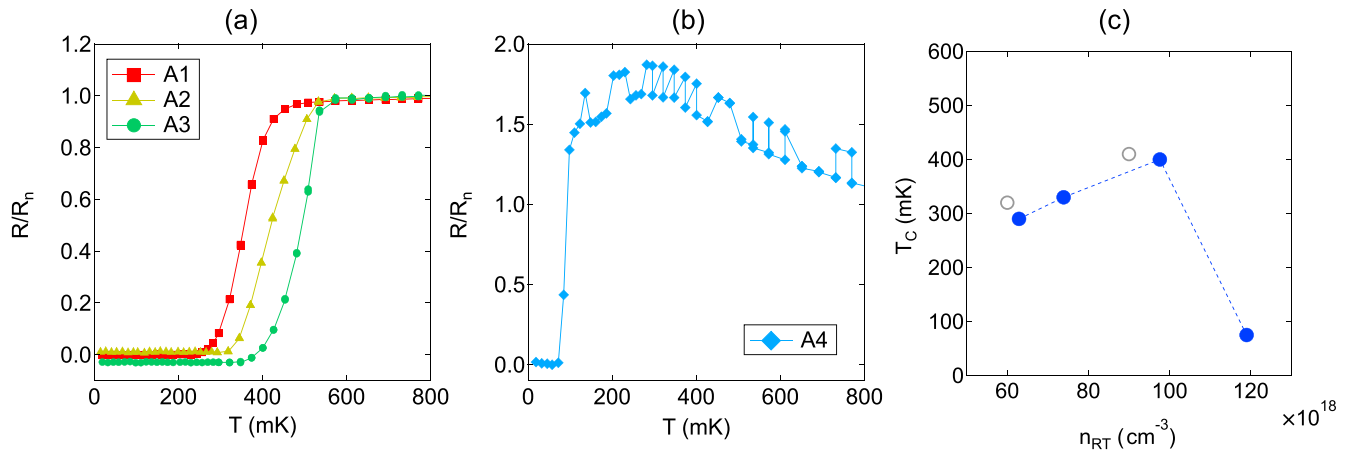


FIG. 3. Normalized resistance R/R_n as a function of temperature for (a) samples A1–A3 and (b) sample A4. The alternating high and low values of R in the normal state are due to artifacts from the lock-in amplifier, and the slight upturn in R before the superconducting transition is occasionally observed in films with nonenhanced T_c . (c) T_c versus n_{RT} for series A films, along with values from comparable Sm:EuTiO₃-capped Sm:SrTiO₃ grown on LSAT from Ref. [23].

are shown in Fig. 3(c), along with values from Sm:EuTiO₃-capped Sm:SrTiO₃ films of comparable thickness from Ref. [23]. The T_c steadily increases with n_{RT} to a maximum of 400 mK in the optimally doped sample with $n_{RT} = 9.8 \times 10^{19} \text{ cm}^{-3}$ (A3), followed by a sharp drop-off of T_c at higher doping densities. The superconducting dome of these 9% Eu samples is similar to that of the superconducting domes exhibited by strained SrTiO₃ in the high-doping regime [21] in that the peak occurs at similar n_{RT} values and a sharp drop-off in T_c is observed on the overdoped side. The T_c 's are also essentially unsuppressed when comparing to strained SrTiO₃ films [gray circles in Fig. 3(c)] [23]. We note that thinner films capped with Sm:EuTiO₃ have generally lower T_c 's than thicker films (see Refs. [21,55]), but all T_c 's are enhanced compared to unstrained Sm:SrTiO₃ films [21]. R/R_n as a function of magnetic field for the series A samples are shown in Fig. 4, and the extracted H_{c2} values are given in Table II along with values

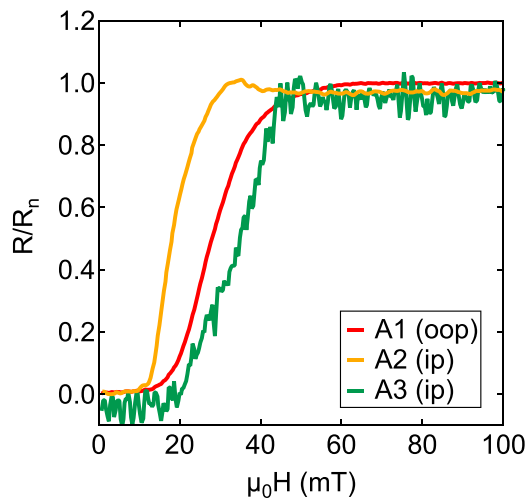


FIG. 4. Critical field measurements for films A1–A3, measured at 20 mK. Measurements were taken by first ramping the field to 0.1 T and then slowly ramping down.

of other previously reported strained Eu_xSr_{1-x}TiO₃ films for comparison [23,36]. As can be seen from Table II, the H_{c2} values for these 9% Eu films are strongly suppressed, even compared to the films with (nominally) 3% Eu [36]. Though H_{c2} measurements for both in-plane (ip) and out of plane (oop) field orientations could not be collected for all samples, the similarity in the oop and ip H_{c2} values suggests that the normally observed anisotropy of H_{c2} in parallel and perpendicular fields for thin film SrTiO₃ has been suppressed.

Normal state transport measurements for series B are shown in Fig. 5. All films were nearly optimally doped with n_{RT} estimated to be $9.8 \times 10^{19} \text{ cm}^{-3}$, $8.3 \times 10^{19} \text{ cm}^{-3}$, and $8.2 \times 10^{19} \text{ cm}^{-3}$ for samples B1, B2, and B3, respectively (sample B1 is the same as sample A3 from series A). Figures 5(a) and 5(b) show $R_s(T)$, which again is qualitatively similar to that of Sm:EuTiO₃-capped Sm:SrTiO₃ films with 0% Eu. The lack of any additional anomalies in $R_s(T)$ would suggest that up to $x = 0.30$ Eu, no spontaneous magnetic ordering occurs. This has also been confirmed by superconducting quantum interference device (SQUID) magnetometry measurements (see Supplemental Material [56]). As can be seen from Fig. 5(c) increasing the Eu content also has a negligible effect on the low-temperature Hall mobility, as the curves essentially fall on top of each other. Figure 5(d) shows n_{3D} as a function of temperature for series B. All films possess similar n_{3D} at elevated temperatures and exhibit carrier depletion beginning around ~ 100 K. As the Eu content increases, the degree of carrier depletion decreases, explaining the different R_s values in Fig. 5(b). The superconducting transitions for series B films are shown in Fig. 6. The T_c of sample B1 (A3) is 400 mK, comparable to that of Sm:EuTiO₃-capped Sm:SrTiO₃ films with 0% Eu, while that of sample B2 is suppressed to ~ 180 mK, and sample B3 does not exhibit a superconducting transition. A summary of series B film properties is given in Table III.

Figure 7(a) shows the SHG intensity measurements scaled by film thickness for the series B films, along with a measurement of a comparable sample structure with 0% Eu shown for comparison (sample A in Refs. [23,55]). A sharp upturn

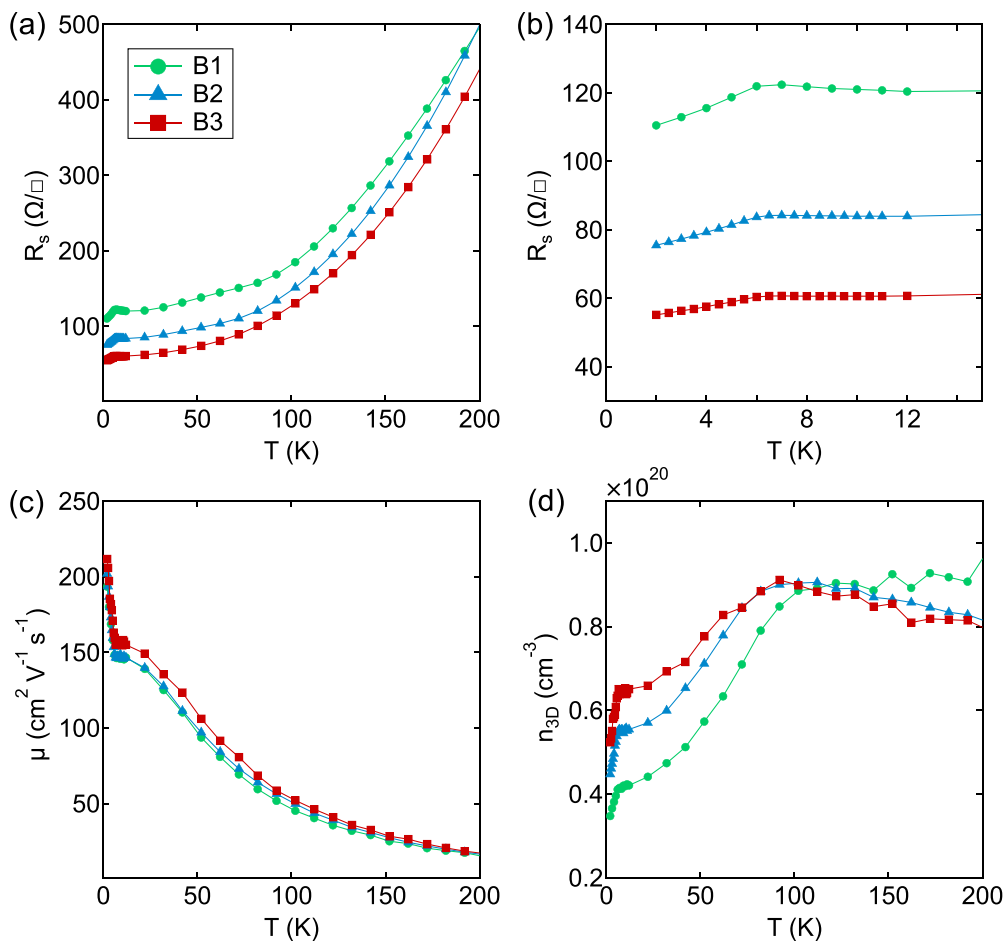
TABLE II. Properties of strained Sm^{3+} -doped $\text{Eu}_x\text{Sr}_{1-x}\text{TiO}_3$ films and heterostructures. The thin capped samples are from Ref. [23] and the thick uncapped Eu-alloyed samples are from Ref. [36].

Thickness (nm)	n_{RT} (cm^{-3})	x (%Eu)	ip H_{c2} (T)	oop H_{c2} (T)	T_c (mK)	Reference
70 ^a	9×10^{19}	0	1.2	0.77	410	[23]
40 ^a	6×10^{19}	0	2.7	1.0	320	[23]
170	8×10^{19}	0.5	1.4	1.0	600	[36]
167	7×10^{19}	2	1.0	0.6	550	[36]
187	5×10^{19}	3	0.6	0.4	500	[36]
68 ^a	6.3×10^{19}	9	–	0.028	290	This work (A1)
92 ^a	7.4×10^{19}	9	0.018	–	330	This work (A2)
75 ^a	9.8×10^{19}	9	0.035	–	400	This work (A3)

^aSamples were capped with ~ 10 nm Sm:EuTiO₃.

in the SHG signal is clearly seen in the 0% Eu sample, whereas the transition is less pronounced in the Eu-alloyed films, although remanences of it still exist. Sharp SHG transitions can be broadened by even a small degree of strain relaxation [32]; however, as can be seen from the XRD data shown in Fig. 7(b), here, all films are fully strained and stoichiometric. Thus, the presence of Eu in concentrations of $x \geq 0.09$ apparently suppresses sharp SHG upturns associ-

ated with a global ferroelectric transition. A persistent finite signal at low temperatures can be attributed to the presence of polar nanodomains, commonly observed in SrTiO₃ films above a ferroelectric transition [26,31,64]. The change in the films' ferroelectric ordering behavior is also indicated by scanning transmission electron microscopy studies, presented in the Supplemental Material [56], which show no polar nanodomains at room temperature for the $x = 0.09$ film, at least


 FIG. 5. Normal state transport properties as a function of temperature for series B. (a) R_s from 200 to 2 K, (b) zoomed-in R_s from 15 to 2 K, (c) mobility, and (d) n_{3D} .

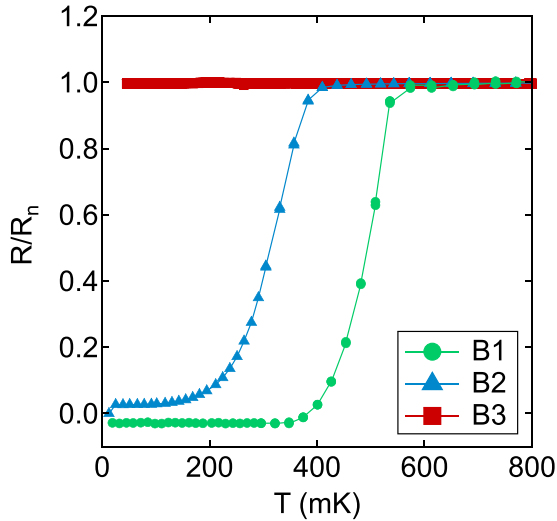


FIG. 6. Superconducting transitions for series B films. Measurements were taken on heating from base temperature. The small offsets of the resistance from zero are measurement artifacts.

within the detection limits of the method, in contrast to a $x = 0$ film.

IV. DISCUSSION

A. Ferroelectric transition

As mentioned in the Introduction, the ferroelectric transition in strained SrTiO_3 has both displacive (soft-mode) [14,65] and order-disorder characteristics, as evidenced by the presence of nanodomains above the transition, which are an essential precursor to the ferroelectric transition [26,31]. The SHG in Fig. 7(a) would indicate that the addition of $x \geq 0.09$ Eu has led to a crossover upon which a long-range ordered state cannot be established, although the steadily increasing SHG signal with decreasing temperature of the moderate-Eu films indicates that the degree of polarization is still increasing. It is reasonable to assume that Eu produces minimal crystalline disorder in SrTiO_3 due to its ionic radius being almost identical to that of Sr, which is supported by the similar crystallinity exhibited by all films in XRD [Fig. 7(a)] and the relatively unchanging normal state transport properties across series B (Fig. 5). Although both SrTiO_3 and EuTiO_3 are considered incipient ferroelectrics due to a soft-mode instability, SrTiO_3 is much closer to its quantum critical point. Studies of $\text{Eu}_x\text{Sr}_{1-x}\text{TiO}_3$ solid solutions have found that the dielectric

TABLE III. Summary of properties for series B samples. The average Eu-Eu distance $l_{\text{Eu-Eu}}$ was calculated using the Eu concentration x as measured by XPS.

Sample	BEP	x	XPS x	n_{RT} (cm^{-3})	$\text{Eu}_x\text{Sr}_{1-x}\text{TiO}_3$	
					film thickness (nm)	T_c (mK)
B1	0.05	0.09	9.8×10^{19}	75	400	8.7
B2	0.10	0.14	8.3×10^{19}	83	180	7.5
B3	0.20	0.30	8.2×10^{19}	92	0	5.8

constant (ϵ') becomes strongly reduced in going from $x = 0$ to $x = 0.2$, and the $\epsilon'(T)$ behavior changes from that of SrTiO_3 , which has a saturating $\epsilon'(T)$ as T approaches 0 K, to relaxor-type behavior with a very broad $\epsilon'(T)$ peak around ~ 30 K [66]. The $0 \leq x \leq 0.25$ range has correspondingly exhibited a strong increase in the frequency of the soft transverse optical phonon mode [67]. This supports the idea that the addition of Eu to the SrTiO_3 host lattice decreases the polarizability and leads to a crossover from a uniform polar ferroelectric ground state to a state with only locally dipolar regions.

B. Superconducting properties

It is rather remarkable that replacing 9% of nonmagnetic Sr^{2+} with magnetic Eu^{2+} results in virtually no suppression of T_c [Fig. 3(c)] and that superconductivity survives up to at least 14%. In an s -wave superconductor, AG theory states that the introduction of magnetic impurities should cause an immediate and continuous suppression of T_c as a function of impurity concentration [37], with typical critical concentrations being on the order of ~ 1 at. % [68]. While the addition of magnetic Eu^{2+} does eventually suppress the T_c , there is thus an initial regime in which it has virtually no effect. In fact, the situation is more analogous to Anderson's theorem for the effect of *non-magnetic* impurities on s -wave superconductors, in which the impurities impose virtually no suppression of T_c up to a certain critical concentration, above which the impurities begin to have larger effects than simply increasing scattering rates [69]. It should be noted, however, that the AG theory tends to hold most strongly for binary and pseudobinary systems. For ternary systems, it has been suggested that the existence of distinct crystallographic sites allows for spatial separation between the conduction electrons and the magnetic sublattice, which could reduce the effect of the exchange interaction [68]. Kondo screening can be a source of resistance to the effect of magnetic impurities. However, Kondo screening is typically manifested by an upturn in resistivity, which we do not see between 2 and 300 K.

Unlike T_c , the magnetic response of the superconducting $x = 0.09$ film does display markedly different behavior from that of doped, strained SrTiO_3 or even $\text{Eu}_x\text{Sr}_{1-x}\text{TiO}_3$ with $x \leq 0.03$. As seen in Table II, though the T_c values at $x = 0.09$ are relatively unsuppressed, the H_{c2} values are suppressed by an order of magnitude (or more) and values are similar to those of bulk SrTiO_3 [70,71]. This suggests a crossover into a different type of superconducting regime associated with the Eu alloying. Interestingly, the suppression of H_{c2} by moderate Eu alloying correlates with the suppression of a global ferroelectric transition. Notably, fully strained films with $x \leq 0.03$ exhibit the signatures of a global ferroelectric transition in SHG along with large H_{c2} values [36]. One possible explanation for enhanced H_{c2} 's at low x is that when ASOC is present due to inversion symmetry breaking, spins are pinned and there will be an additional energy cost for pair breaking for certain magnetic field orientations [41]. As the long-range ordered ferroelectric state is lost, any enhancement of H_{c2} by ASOC would then diminish. At this point, however, this suggestion is purely speculative. We also note that both ip and oop H_{c2} 's are reduced in magnitude while the effect of ASOC on H_{c2} should be strongly directional.

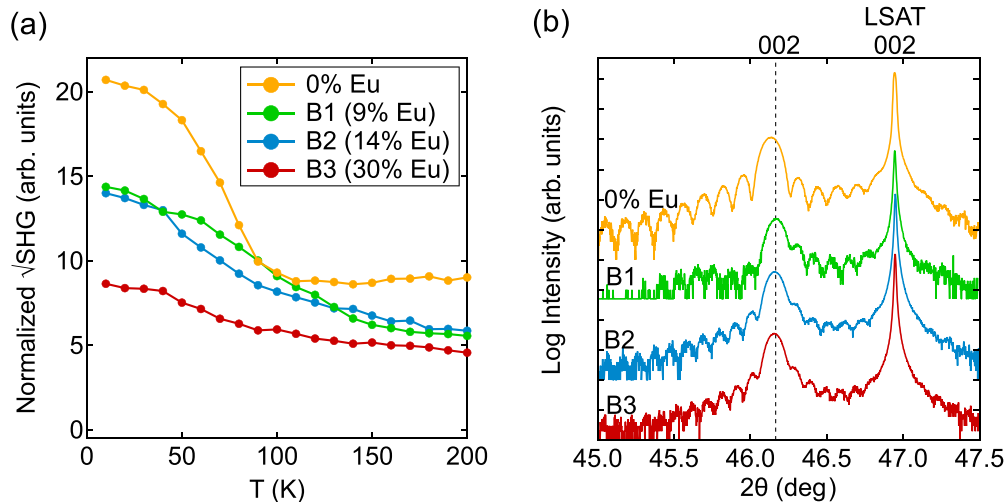


FIG. 7. (a) Square root of SHG signal intensity normalized to film thickness as a function of temperature for series B, alongside a comparable Sm:EuTiO₃/Sm:SrTiO₃/LSAT heterostructure, which displays the signatures of a global ferroelectric transition (sample A from Ref. [23]). (b) On-axis XRD scans for series B, along with scan of the 0% Eu sample in (a).

V. CONCLUSIONS

We have shown that films of Sm-doped Eu_xSr_{1-x}TiO₃ remain superconducting up to Eu concentrations of at least $x = 0.14$. The crossover from formation of a long-range ferroelectric state induced by strain to one that contains only locally polar order is supported by the suppression of a strong upturn in SHG intensity. The strongly suppressed H_{c2} 's in this regime suggest that the long-range polar phase may provide protection from magnetic depairing, which is lost when the polar domains become randomly oriented, adding to the growing evidence that polar order influences the superconductivity of SrTiO₃. The eventual total suppression of superconductivity in the range $0.14 < x < 0.30$ may also be connected to the suppression of polar order, but at this point we can only speculate. The results show, however, that suppressing ferroelectricity, i.e., driving the films closer to a putative quantum critical point, in this case via Eu alloying, does not promote superconductivity, contrary to the suggestions of some of the theoretical proposals. There are very few theories that directly connect superconductivity to spin-orbit coupling [72,73], although there are recent suggestions of a more indirect link via a modification of the phonon coupling [8].

We hope that the results motivate further theoretical studies on the role of static polar order in the superconductivity of SrTiO₃.

ACKNOWLEDGMENTS

This work was mainly supported by the U.S. Department of Energy (Award No. DE-SC0020305). Microscopy studies were supported by the U.S. Department of Energy (Award No. DEFG02-02ER45994). Partial support was also provided by a MURI program of the Army Research Office (Grant No. W911NF-16-1-0361). N.G.C. and L.K. acknowledge support through the UCSB Quantum Foundry, which is supported by the National Science Foundation (Award No. DMR-1906325). T.N.P. acknowledges the U.S. National Science Foundation Graduate Research Fellowship Program for support (Award No. 1650114). Optical second harmonic generation measurements were supported by the National Science Foundation (Award No. DMR-2140786). The work made use of the MRL Shared Experimental Facilities, which are supported by the MRSEC Program of the U.S. National Science Foundation under Award No. DMR 1720256.

- [1] J. F. Schooley, W. R. Hosler, and M. L. Cohen, Superconductivity in Semiconducting SrTiO₃, *Phys. Rev. Lett.* **12**, 474 (1964).
- [2] M. N. Gastiasoro, J. Ruhman, and R. M. Fernandes, Superconductivity in dilute SrTiO₃: A review, *Ann. Phys.* **417**, 168107 (2020).
- [3] C. S. Koonce, M. L. Cohen, J. F. Schooley, W. R. Hosler, and E. R. Pfeiffer, Superconducting transition temperatures of semiconducting strontium titanate, *Phys. Rev.* **163**, 380 (1967).
- [4] K. A. Müller and H. Burkard, SrTiO₃: An intrinsic quantum paraelectric below 4 K, *Phys. Rev. B* **19**, 3593 (1979).
- [5] S. E. Rowley, C. Enderlein, J. F. de Oliveira, D. A. Tompsett, E. B. Saitovitch, S. S. Saxena, and G. G. Lonzarich, Superconductivity in the vicinity of a ferroelectric quantum phase transition, [arXiv:1801.08121](https://arxiv.org/abs/1801.08121).
- [6] Y. Kedem, Novel pairing mechanism for superconductivity at a vanishing level of doping driven by critical ferroelectric modes, *Phys. Rev. B* **98**, 220505(R) (2018).
- [7] J. M. Edge, Y. Kedem, U. Aschauer, N. A. Spaldin, and A. V. Balatsky, Quantum Critical Origin of the Superconducting Dome in SrTiO₃, *Phys. Rev. Lett.* **115**, 247002 (2015).
- [8] M. N. Gastiasoro, T. V. Trevisan, and R. M. Fernandes, Anisotropic superconductivity mediated by ferroelectric fluctuations in cubic systems with spin-orbit coupling, *Phys. Rev. B* **101**, 174501 (2020).
- [9] C. Enderlein, J. F. de Oliveira, D. A. Tompsett, E. B. Saitovitch, S. S. Saxena, G. G. Lonzarich, and S. E. Rowley, Superconductivity mediated by polar modes in ferroelectric metals, *Nat. Commun.* **11**, 4852 (2020).

- [10] J. G. Bednorz and K. A. Müller, $\text{Sr}_{1-x}\text{Ca}_x\text{TiO}_3$: An XY Quantum Ferroelectric with Transition to Randomness, *Phys. Rev. Lett.* **52**, 2289 (1984).
- [11] C. W. Rischau, X. Lin, C. P. Grams, D. Finck, S. Harms, J. Engelmayr, T. Lorenz, Y. Gallais, B. Fauque, J. Hemberger, and K. Behnia, A ferroelectric quantum phase transition inside the superconducting dome of $\text{Sr}_{1-x}\text{Ca}_x\text{TiO}_{3-\delta}$, *Nat. Phys.* **13**, 643 (2017).
- [12] K. Bethe and F. Welz, Preparation and properties of (Ba, Sr)TiO₃ single crystals, *Mater. Res. Bull.* **6**, 209 (1971).
- [13] M. Itoh, R. Wang, Y. Inaguma, T. Yamaguchi, Y. J. Shan, and T. Nakamura, Ferroelectricity Induced by Oxygen Isotope Exchange in Strontium Titanate Perovskite, *Phys. Rev. Lett.* **82**, 3540 (1999).
- [14] H. Uwe and T. Sakudo, Stress-induced ferroelectricity and soft phonon modes in SrTiO₃, *Phys. Rev. B* **13**, 271 (1976).
- [15] N. A. Pertsev, A. K. Tagantsev, and N. Setter, Phase transitions and strain-induced ferroelectricity in SrTiO₃ epitaxial thin films, *Phys. Rev. B* **61**, R825 (2000).
- [16] J. H. Haeni, P. Irvin, W. Chang, R. Uecker, P. Reiche, Y. L. Li, S. Choudhury, W. Tian, M. E. Hawley, B. Craigo, A. K. Tagantsev, X. Q. Pan, S. K. Streiffer, L. Q. Chen, S. W. Kirchoefer, J. Levy, and D. G. Schlom, Room-temperature ferroelectricity in strained SrTiO₃, *Nature (London)* **430**, 758 (2004).
- [17] A. Stucky, G. W. Scheerer, Z. Ren, D. Jaccard, J. M. Poumirol, C. Barreateau, E. Giannini, and D. van der Marel, Isotope effect in superconducting *n*-doped SrTiO₃, *Sci. Rep.* **6**, 37582 (2016).
- [18] Y. Tomioka, N. Shirakawa, and I. H. Inoue, Superconductivity enhanced in the polar metal region of $\text{Sr}_{0.95}\text{Ba}_{0.05}\text{TiO}_3$ and $\text{Sr}_{0.985}\text{Ca}_{0.015}\text{TiO}_3$ revealed by systematic Nb doping, *npj Quantum Mater.* **7**, 111 (2022).
- [19] Y. Tomioka, N. Shirakawa, K. Shibuya, and I. H. Inoue, Enhanced superconductivity close to a non-magnetic quantum critical point in electron-doped strontium titanate, *Nat. Commun.* **10**, 738 (2019).
- [20] C. Herrera, J. Cerbin, A. Jayakody, K. Dunnett, A. V. Balatsky, and I. Sochnikov, Strain-engineered interaction of quantum polar and superconducting phases, *Phys. Rev. Mater.* **3**, 124801 (2019).
- [21] K. Ahadi, L. Galletti, Y. Li, S. Salmani-Rezaie, W. Wu, and S. Stemmer, Enhancing superconductivity in SrTiO₃ films with strain, *Sci. Adv.* **5**, eaaw0120 (2019).
- [22] R. Russell, N. Ratcliff, K. Ahadi, L. Y. Dong, S. Stemmer, and J. W. Harter, Ferroelectric enhancement of superconductivity in compressively strained SrTiO₃ films, *Phys. Rev. Mater.* **3**, 091401(R) (2019).
- [23] H. Jeong, R. Russell, N. G. Combs, T. N. Pardue, J. W. Harter, and S. Stemmer, Similarity in the critical thicknesses for superconductivity and ferroelectricity in strained SrTiO₃ films, *Appl. Phys. Lett.* **121**, 012601 (2022).
- [24] K. A. Müller, W. Berlinger, and E. Tosatti, Indication for a novel phase in the quantum paraelectric regime of SrTiO₃, *Z. Phys. B* **84**, 277 (1991).
- [25] E. K. H. Salje, O. Aktas, M. A. Carpenter, V. V. Laguta, and J. F. Scott, Domains within Domains and Walls within Walls: Evidence for Polar Domains in Cryogenic SrTiO₃, *Phys. Rev. Lett.* **111**, 247603 (2013).
- [26] S. Salmani-Rezaie, K. Ahadi, W. M. Strickland, and S. Stemmer, Order-Disorder Ferroelectric Transition of Strained SrTiO₃, *Phys. Rev. Lett.* **125**, 087601 (2020).
- [27] B. Zalar, A. Lebar, J. Seliger, R. Blinc, V. V. Laguta, and M. Itoh, NMR study of disorder in BaTiO₃ and SrTiO₃, *Phys. Rev. B* **71**, 064107 (2005).
- [28] H. Uwe, H. Yamaguchi, and T. Sakudo, Ferroelectric microregion in $\text{KTa}_{1-x}\text{Nb}_x\text{O}_3$ and SrTiO₃, *Ferroelectrics* **96**, 123 (1989).
- [29] H. W. Jang, A. Kumar, S. Denev, M. D. Biegalski, P. Maksymovych, C. W. Bark, C. T. Nelson, C. M. Folkman, S. H. Baek, N. Balke, C. M. Brooks, D. A. Tenne, D. G. Schlom, L. Q. Chen, X. Q. Pan, S. V. Kalinin, V. Gopalan, and C. B. Eom, Ferroelectricity in Strain-Free SrTiO₃ Thin Films, *Phys. Rev. Lett.* **104**, 197601 (2010).
- [30] U. Bianchi, W. Kleemann, and J. G. Bednorz, Raman scattering of ferroelectric $\text{Sr}_{1-x}\text{Ca}_x\text{TiO}_3$, $x = 0.007$, *J. Phys.: Condens. Matter* **6**, 1229 (1994).
- [31] S. Salmani-Rezaie, K. Ahadi, and S. Stemmer, Polar nanodomains in a ferroelectric superconductor, *Nano Lett.* **20**, 6542 (2020).
- [32] S. Salmani-Rezaie, H. Jeong, R. Russell, J. W. Harter, and S. Stemmer, Role of locally polar regions in the superconductivity of SrTiO₃, *Phys. Rev. Mater.* **5**, 104801 (2021).
- [33] M. Kim, Y. Kozuka, C. Bell, Y. Hikita, and H. Y. Hwang, Intrinsic spin-orbit coupling in superconducting delta-doped SrTiO₃ heterostructures, *Phys. Rev. B* **86**, 085121 (2012).
- [34] Y. Ayino, J. Yue, T. Wang, Bharat Jalan, and V. S. Prihadi, Effects of paramagnetic pair-breaking and spin-orbital coupling on multi-band superconductivity, *J. Phys.: Condens. Matter* **32**, 38LT02 (2020).
- [35] T. Schumann, L. Galletti, H. Jeong, K. Ahadi, W. M. Strickland, S. Salmani-Rezaie, and S. Stemmer, Possible signatures of mixed-parity superconductivity in doped polar SrTiO₃ films, *Phys. Rev. B* **101**, 100503(R) (2020).
- [36] S. Salmani-Rezaie, L. Galletti, T. Schumann, R. Russell, H. Jeong, Y. Li, J. W. Harter, and S. Stemmer, Superconductivity in magnetically doped SrTiO₃, *Appl. Phys. Lett.* **118**, 202602 (2021).
- [37] A. A. Abrikosov and L. P. Gor'kov, Contribution to the theory of superconducting alloys with paramagnetic impurities, *Zh. Eksp. Teor. Fiz.* **39**, 1781 (1961) [*Sov. Phys. JETP* **12**, 1243 (1961)].
- [38] J. M. Edge and A. V. Balatsky, Upper critical field as a probe for multiband superconductivity in bulk and interfacial STO, *J. Supercond. Novel Magn.* **28**, 2373 (2015).
- [39] M. S. Scheurer, M. Hoyer, and J. Schmalian, Pair breaking in multiorbital superconductors: An application to oxide interfaces, *Phys. Rev. B* **92**, 014518 (2015).
- [40] L. P. Gor'kov and E. I. Rashba, Superconducting 2D System with Lifted Spin Degeneracy: Mixed Singlet-Triplet State, *Phys. Rev. Lett.* **87**, 037004 (2001).
- [41] M. Smidman, M. B. Salamon, H. Q. Yuan, and D. F. Agterberg, Superconductivity and spin-orbit coupling in non-centrosymmetric materials: A review, *Rep. Prog. Phys.* **80**, 036501 (2017).
- [42] S. Fujimoto, Electron correlation and pairing states in superconductors without inversion symmetry, *J. Phys. Soc. Jpn.* **76**, 051008 (2007).
- [43] O. G. Dimitrova and M. V. Feigel'man, Theory of a two-dimensional superconductor with broken inversion symmetry, *Phys. Rev. B* **76**, 014522 (2007).

- [44] H. Nam, H. Chen, T. J. Liu, J. Kim, C. D. Zhang, J. Yong, T. R. Lemberger, P. A. Kratz, J. R. Kirtley, K. Moler, P. W. Adams, A. H. MacDonald, and C. K. Shih, Ultrathin two-dimensional superconductivity with strong spin-orbit coupling, *Proc. Natl. Acad. Sci. USA* **113**, 10513 (2016).
- [45] K. Michaeli, A. C. Potter, and P. A. Lee, Superconducting and Ferromagnetic Phases in SrTiO₃/LaAlO₃ Oxide Interface Structures: Possibility of Finite Momentum Pairing, *Phys. Rev. Lett.* **108**, 117003 (2012).
- [46] A. D. Caviglia, M. Gabay, S. Gariglio, N. Reyren, C. Cancellieri, and J. M. Triscone, Tunable Rashba Spin-Orbit Interaction at Oxide Interfaces, *Phys. Rev. Lett.* **104**, 126803 (2010).
- [47] P. K. Rout, E. Maniv, and Y. Dagan, Link between the Superconducting Dome and Spin-Orbit Interaction in the (111) LaAlO₃/SrTiO₃ Interface, *Phys. Rev. Lett.* **119**, 237002 (2017).
- [48] D. Stornaiuolo, D. Massarotti, R. Di Capua, P. Lucignano, G. P. Pepe, M. Salluzzo, and F. Tafuri, Signatures of unconventional superconductivity in the LaAlO₃/SrTiO₃ two-dimensional system, *Phys. Rev. B* **95**, 140502(R) (2017).
- [49] M. S. Scheurer and J. Schmalian, Topological superconductivity and unconventional pairing in oxide interfaces, *Nat. Commun.* **6**, 6005 (2015).
- [50] S. Kanasugi and Y. Yanase, Spin-orbit-coupled ferroelectric superconductivity, *Phys. Rev. B* **98**, 024521 (2018).
- [51] S. Kanasugi and Y. Yanase, Multiorbital ferroelectric superconductivity in doped SrTiO₃, *Phys. Rev. B* **100**, 094504 (2019).
- [52] J. H. Lee, L. Fang, E. Vlahos, X. L. Ke, Y. W. Jung, L. F. Kourkoutis, J. W. Kim, P. J. Ryan, T. Heeg, M. Roeckerath, V. Goian, M. Bernhagen, R. Uecker, P. C. Hammel, K. M. Rabe, S. Kamba, J. Schubert, J. W. Freeland, D. A. Muller, C. J. Fennie *et al.*, A strong ferroelectric ferromagnet created by means of spin-lattice coupling, *Nature (London)* **466**, 954 (2010).
- [53] B. Jalan, R. Engel-Herbert, N. J. Wright, and S. Stemmer, Growth of high-quality SrTiO₃ films using a hybrid molecular beam epitaxy approach, *J. Vac. Sci. Technol. A* **27**, 461 (2009).
- [54] K. Ahadi, L. Galletti, and S. Stemmer, Evidence of a topological Hall effect in Eu_{1-x}Sm_xTiO₃, *Appl. Phys. Lett.* **111**, 172403 (2017).
- [55] H. Jeong, N. G. Combs, S. Munyan, A. Rashidi, and S. Stemmer, Reducing surface depletion of superconducting SrTiO₃ films with EuTiO₃ capping layers, *Appl. Phys. Lett.* **119**, 162601 (2021).
- [56] See Supplemental Material at <http://link.aps.org/supplemental/10.1103/PhysRevB.107.094504> for XRD data from uncapped films, a reciprocal space map, XPS data, studies of film degradation, STEM data, and results from magnetization measurements, which includes Refs. [57–62].
- [57] L. Sagarna, S. Populoh, A. Shkabko, J. Eilertsen, A. E. Maegli, R. Hauert, M. Schrade, L. Karvonen, and A. Weidenkaff, Influence of the oxygen content on the electronic transport properties of Sr_xEu_{1-x}TiO_{3-δ}, *J. Phys. Chem. C* **118**, 7821 (2014).
- [58] B. A. Orlowski, S. Mickievicius, V. Osinniy, A. J. Nadolny, B. Taliashvili, P. Dziawa, T. Story, R. Medicherla, and W. Drube, High-energy x-ray photoelectron spectroscopy study of MBE grown (Eu, Gd) Te layers, *Nucl. Instr. Methods Phys. Res., Sect. B* **238**, 346 (2005).
- [59] T. Chatterjee, P. J. McCann, X. M. Fang, and M. B. Johnson, Eu:CaF₂ layers on *p*-Si (100) grown using molecular beam epitaxy as materials for Si-based optoelectronics, *J. Vac. Sci. Technol. B* **16**, 1463 (1998).
- [60] A. Ney, T. Kammermeier, V. Ney, K. Ollefs, and S. Ye, Limitations of measuring small magnetic signals of samples deposited on a diamagnetic substrate, *J. Magn. Magn. Mater.* **320**, 3341 (2008).
- [61] M. Buchner, K. Hoffer, B. Henne, V. Ney, and A. Ney, Tutorial: Basic principles, limits of detection, and pitfalls of highly sensitive SQUID magnetometry for nanomagnetism and spintronics, *J. Appl. Phys.* **124**, 161101 (2018).
- [62] L. M. C. Pereira, J. P. Araujo, M. J. Van Bael, K. Temst, and A. Vantomme, Practical limits for detection of ferromagnetism using highly sensitive magnetometry techniques, *J. Phys. D* **44**, 215001 (2011).
- [63] T. Katsufuji and Y. Tokura, Transport and magnetic properties of a ferromagnetic metal: Eu_{1-x}R_xTiO₃, *Phys. Rev. B* **60**, R15021 (1999).
- [64] R. C. Haislmaier, R. Engel-Herbert, and V. Gopalan, Stoichiometry as key to ferroelectricity in compressively strained SrTiO₃ films, *Appl. Phys. Lett.* **109**, 032901 (2016).
- [65] A. Antons, J. B. Neaton, K. M. Rabe, and D. Vanderbilt, Tunability of the dielectric response of epitaxially strained SrTiO₃ from first principles, *Phys. Rev. B* **71**, 024102 (2005).
- [66] R. Muralidharan, K. Meera, and Y. H. Jeong, Evidence on the quantum critical point in EuTiO₃ – SrTiO₃ solid solution, *Phys. B (Amsterdam)* **620**, 413225 (2021).
- [67] Z. Guguchia, A. Shengelaya, H. Keller, J. Köhler, and A. Bussmann-Holder, Tuning the structural instability of SrTiO₃ by Eu doping: The phase diagram of Sr_{1-x}Eu_xTiO₃, *Phys. Rev. B* **85**, 134113 (2012).
- [68] C. T. Wolowiec, B. D. White, and M. B. Maple, Conventional magnetic superconductors, *Phys. C (Amsterdam)* **514**, 113 (2015).
- [69] P. W. Anderson, Theory of dirty superconductors, *J. Phys. Chem. Solids* **11**, 26 (1959).
- [70] C. Collignon, B. Fauqué, A. Cavanna, U. Gennser, D. Mailly, and K. Behnia, Superfluid density and carrier concentration across a superconducting dome: The case of strontium titanate, *Phys. Rev. B* **96**, 224506 (2017).
- [71] H. Suzuki, H. Bando, Y. Ootuka, I. H. Inoue, T. Yamamoto, K. Takahashi, and Y. Nishihara, Superconductivity in single-crystalline Sr_{1-x}La_xTiO₃, *J. Phys. Soc. Jpn.* **65**, 1529 (1996).
- [72] Y. Gindikin and V. A. Sablikov, Electron correlations due to pair spin-orbit interaction in 2D electron systems, *Phys. E (Amsterdam)* **143**, 115328 (2022).
- [73] J. Hutchinson, J. E. Hirsch, and F. Marsiglio, Enhancement of superconducting T_c due to the spin-orbit interaction, *Phys. Rev. B* **97**, 184513 (2018).